Dalton Transactions

Accepted Manuscript

ROYAL SOCIETY OF CHEMISTRY

www.rsc.org/dalton

Photocatalytic Property of Bi_2O_3 Nanoparticle Modified BiOCl Composite with a Nanolayered Hierarchical Structure Synthesized by In Situ Reactions

Jiajia Hu[1], Guangqing Xu[1*], Jinwen Wang[1], Jun Lv[1], Xinyi Zhang[2], Ting Xie[3], Zhixiang Zheng[1], Yucheng Wu[1, 2*]

1 Laboratory of Functional Nanomaterials and Devices, School of Materials Science and Engineering, Hefei University of Technology, Hefei 230009, China

2 Anhui Provincial Key Laboratory of Advanced Functional Materials and Devices, Hefei University of Technology, Hefei 230009, China.

3 Institute of Tribology, Hefei University of Technology, Hefei 230009, China.

Abstrat: A Bi_2O_3 nanoparticle modified BiOCl composite was synthesized by solvothermal method combined with in situ reduction and oxidation in KBH_4 and H_2O_2 solutions respectively. The thickness of BiOCl nanosheet and amount of Bi_2O_3 nanoparticle can be adjusted by changing KBH_4 concentration. The structure, morphology, elemental composition and optical absorption performance were characterized by using X-ray diffraction diffractometer, scanning electron microscope, high resolution transmission electron microscope, X-ray photoelectron spectroscope and UV-Vis diffuse reflection spectroscope respectively. A nanolayered hierarchical structure of BiOCl was observed, and Bi_2O_3 nanoparticles were found to be evenly distributed on the surface/interface of the nanosheets. The photocatalytic activity of the composite was tested by the degradation of 40 $mg \cdot L^{-1}$ methyl orange solution under UV light illumination. The Bi_2O_3/BiOCl composite prepared in a KBH_4 concentration of 0.02 M achieved the highest photocatalytic rate of 95.7% in 8 min under UV light illumination with a kinetic constant of 0.3125 1/min. The photocatalytic mechanism of the composite has been discussed.

Keywords: BiOCl nanosheet; Bi_2O_3 nanoparticle; Hierarchical Structure; Heterojunction; Photocatalysis

1 Introduction

With the consumption of traditional fossil fuels, the contamination caused by waste gases, organic molecule pollutants and biological substances has been becoming a severe environmental problem of worldwide concern. Many methods including physical and chemical treatments, such as adsorption, ultrafiltration, UV radiation, photocatalytic degradation, enzymatic technology and etc., have been applied for removing the organic pollutants [1]. Among them, photocatalytic degradation of organics based on using semiconductors has attracted considerable attention in the environment protection due to the characteristics of semiconductors, which can transform the solar energy to catalytic active electron-hole pairs.

* Corresponding author: Tel.: +86 551 62901372
Email address: gqxu1979@hfut.edu.cn (Guangqing Xu)
ycwu@hfut.edu.cn (Yucheng Wu)

Bismuth oxyhalides (BiOX, X=Cl, Br, I), as a category of Bi-based semiconductors, exhibit promising applications in photocatalysis due to their outstanding optical and electrical properties [2-5]. Although the band gap energy of BiOCl is about 3.4 eV, which is wider than that of TiO_2, the photocatalytic property of BiOCl is better than that of TiO_2. Zhang's group [6] reported a better photocatalytic performance of BiOCl than that of commercial P25 toward methyl orange (MO) degradation under UV light illumination. The superior photocatalytic performance of BiOCl can be ascribed to the unique layered structure of BiOCl composed of $[Bi_2O_2]$ slabs interleaved with double halogen atom slabs along the [001] direction [7, 8]. The layered structure possesses enough space to polarize the corresponding atoms and atomic orbital, and the induced dipole moment can separate the photoinduced electrons and holes effectively [9], resulting in the high photocatalytic activities of BiOCl.

Many researches have been focused on the synthesis and modification of BiOCl nano/micro-structures to enhance their photocatalytic performance. Recently, a variety of BiOCl nano/micro-structures, such as nanosheets [10-12], self-assembled microsphere [13, 14] and one dimensional nanowires [15] have been studied on their photocatalytic property. For further promoting the photocatalytic performances of BiOCl or achieving the visible light activity, coupling with other materials to construct heterojunctions has been a more effective approach, such as metal nanoparticles [16-18] and semiconductor quantum dots [19-21]. The heterojunctions can separate the photogenerated electron-hole pairs by controlling chargers' transfer, resulting in the enhancement of photocatalytic performance. In most cases, these heterojunctions were reported to be formed by depositing the nanoparticles on the surface of BiOCl from outside, resulting in a higher contact resistance of the interface, which is adverse to the separation of the photogenerated electron-hole pairs.

In this study, Bi_2O_3 nanoparticles were deposited on the surface/interface of BiOCl nanosheets with nanolayered hierarchical structure by in situ reactions, which possesses better combination and lattice matching between the nanoparticle and the nanosheet. Higher surface area, higher UV light absorption and higher separation effect to the electron-hole pairs of Bi_2O_3/BiOCl composite due to its Nanolayered hierarchical structure and the heterojunctions resulted in the enhancement of photocatalytic performances.

2 Experimental

2.1 Chemicals

Bismuth nitrate pentahydrate ($Bi(NO_3)_3 \cdot 5H_2O$), sodium chloride (NaCl), ethylene glycol (EG), KBH_4, H_2O_2, benzoquinone (BQ), NaI, isopropanol (IPA) were purchased from Sinopharm Chemical Reagent Co., Ltd. (Shanghai, China). All reagents were analytical grade and used as received without

further purification.

2.2 Synthesis

BiOCl were synthesized via solvothermal method. In a typical procedure, 2 mmol $Bi(NO_3)_3 \cdot 5H_2O$ was dissolved in 25 mL EG, and 2 mmol NaCl was dissolved in 25 mL deionized water. The NaCl aqueous solution was added dropwise into $Bi(NO_3)_3$ solution with continuous stirring. After being stirred for 30 min, the mixed solution was transferred to a Teflon-lined stainless autoclave. The solvothermal synthesis was performed at 150℃ for 10 h in an electric oven. The resulted precipitate was centrifuged and washed with ethanol and deionized water several times to remove the chemical remnants. Finally, the white BiOCl powders was obtained by drying the precipitate at 40℃ in air.

Bi_2O_3 deposition was performed via in situ reduction and oxidation of BiOCl powders in KBH_4 and H_2O_2 solutions, respectively. 0.5 g BiOCl powder was added into 40 mL KBH_4 solutions with different KBH_4 concentrations ranging from 10 to 50 mM respectively, and reacted for 10 min with continuous stirring. The products were washed with deionized water several times to remove the chemical remnants. The resulted products were then put into a 40 mL H_2O_2 aqueous solution with a H_2O_2 concentration of 15%, and reacted for 30 min with ultrasonication. The resulted precipitate was washed with deionized water several times to remove the chemical remnants. The final Bi_2O_3/BiOCl composite was obtained by drying the precipitate at 40℃ in air. The Bi_2O_3/BiOCl composite prepared with different KBH_4 concentrations of 0.01 M, 0.02 M, 0.03 M, 0.04 M and 0.05 M were labeled as Bi_2O_3/BiOCl-0.01, Bi_2O_3/BiOCl-0.02, Bi_2O_3/BiOCl-0.03, Bi_2O_3/BiOCl-0.04 and Bi_2O_3/BiOCl-0.05, respectively.

2.3 Characterization

The phase structure of the samples was measured by an X-ray diffraction meter (XRD, D/MAX2500V) using Cu Kα radiation with 2θ ranging from 10° to 70°. Morphologies of the samples were observed with a SU8020 field emission scanning electron microscope (FESEM) and a JEM-2100F high resolution transmission electron microscope (HRTEM). The HRTEM samples were prepared by dispersing the powder in ethyl alcohol with ultrasonication for 20 min, and carbon-coated copper grids were used as sample holders. X-Ray photoelectron spectroscopy (XPS) analysis on the samples was performed using an ESCALAB 250 photoelectron spectrometer using a monochromatic Al Ka X-ray beam (1486.60 eV). The optical absorption performance of the samples was evaluated by a diffuse reflectance spectrometer (UV3600, Shimadzu) using $BaSO_4$ as reference.

2.4 Photocatalysis

Photocatalytic degradation of MO solution was used to evaluate the photocatalytic property of the

samples, and the photocatalytic tests were conducted on an XPA-7 photochemical reactor (Nanjing Xujiang Machine-electronic Company, China) using a 300 W high-pressure mercury lamp as the UV light source (maximum emission wavelength at 365 nm in the UV region). An optical filter with cutoff wavelength at 400 nm was used to eliminate the visible light. The distance between the solution and the lamp was kept at 10 cm, and the solution was continuous stirred during the photocatalytic degradation process.

In a typical procedure, 0.01 g photocatalyst was put into 10 mL MO solution with a concentration of 40 $mg \cdot L^{-1}$. The suspension was vigorously stirred for 30 min in the dark to achieve the adsorption/desorption equilibrium. After being illuminated successively for 2, 4, 6 and 8 min, a 5 mL solution was collected from the suspension and was centrifuged, then the upper clear solution was measured by a UV1800 spectrometer (Shimadzu, Japan) to record the remnant concentration of MO in the solution after being photodegraded.

For further studying the effect of the active species of h^+, $\cdot O_2^-$ and HO· on the photocatalytic performance of BiOCl and Bi_2O_3/BiOCl, three sacrificial agents of NaI, BQ and IPA with concentration of 10 mM were added respectively in the MO solution. The change of degradation rates reflects the roles of the corresponding active species on the photocatalytic property of the composite.

3 Result and discussion

3.1 Characterizations

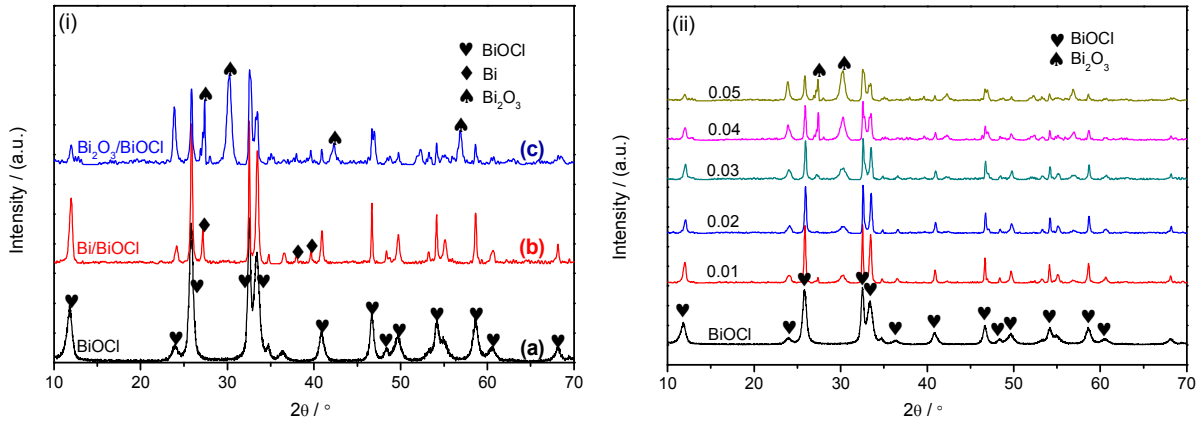

Fig.1 XRD patterns of BiOCl and modified BiOCl. (i) XRD patterns of BiOCl and the products after being reduced and oxidized, (ii) XRD patterns of Bi_2O_3/BiOCl composite synthesized in KBH_4 solutions with different concentrations.

Fig.1 shows the XRD patterns of BiOCl and the modified BiOCl, reflecting the phase structure of samples during the synthesis process. Fig.1 (i) shows the XRD patterns of as-prepared BiOCl sample and the product after being in situ reduced and oxidized. The hydrothermal products possess the

tetragonal BiOCl phase structure (JCPDS File No.06-0249) as shown in curve (a). There is no detectable change of the BiOCl phase structure in the products after being in situ reduced and oxidized, as shown by its characteristic diffraction peaks in curve (b) and (c), indicating that the successive reduction and oxidation processes do not affect the crystal structure of BiOCl. Some new diffraction peaks at 27.1º, 37.9º and 39.6º can be observed in curve (b) in addition to the diffraction peaks appeared in BiOCl nanosheets, which are corresponding to the (012), (104) and (110) crystal planes of metallic Bi (JCPDS File No. 44-1246) respectively, indicating that BiOCl is partly reduced to metallic Bi, and BiOCl deposited with Bi is achieved. The following oxidation of Bi/BiOCl in H_2O_2 solution results in the disappearance of the diffraction peaks originated from metallic Bi and the appearance of new diffraction peaks at 27.35º, 30.2º, 42.3º and 52.3º corresponding to the (310), (222), (332) and (433) crystal planes of Bi_2O_3 (JCPDS File NO. 45-1344) respectively, indicating that metallic Bi is oxidized to Bi_2O_3 phase.

Fig.1 (ii) shows the XRD patterns of Bi_2O_3/BiOCl composites synthesized in KBH_4 solutions with different concentrations ranging from 10 mM to 50 mM. From the comparison of the characteristic diffraction peaks at 25.8º (BiOCl) and 30.2º (Bi_2O_3), the peak intensity of BiOCl becomes weaker and that of Bi_2O_3 goes stronger with the increase of KBH_4 concentration, which means that the amount of Bi_2O_3 in Bi_2O_3/BiOCl composites is adjustable via changing the concentration of KBH_4. The similar full width at half maximum (FWHM) of diffraction peak at 30.2º (~0.678º) for the composites synthesized with different concentrations of KBH_4 indicates a similar grain size of Bi_2O_3 in different Bi_2O_3/BiOCl samples.

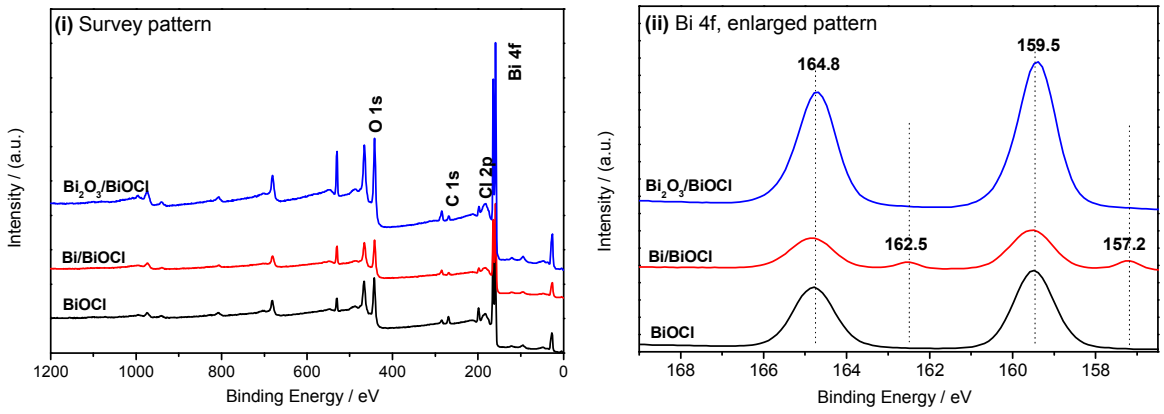

Fig.2 XPS patterns of BiOCl, Bi/BiOCl and Bi_2O_3/BiOCl. (i) Survey pattern, (ii) high resolution pattern of Bi 4f electrons.

Fig.2 shows the XPS patterns of BiOCl, Bi/BiOCl and Bi_2O_3/BiOCl to reveal the elemental compositions of these samples. The survey patterns of as-prepared BiOCl and BiOCl after being in situ reduced and oxidized are shown in Fig.2 (i). The main element compositions of the samples are

Bi, O and Cl with the binding energy peaks at 163 eV (Bi 4f), 442 eV (O 1s) and 198 eV (Cl 2p) respectively. The peak of C 1s at 284.7 eV exists in all samples and is originated from the testing process. The high-resolution XPS patterns of the three samples in the narrow region of Bi 4f are shown in Fig.2 (ii). Double peaks with the binding energy of 159.5 and 164.8 eV can be observed in the pattern of as-prepared BiOCl sample with, corresponding to the 4f 7/2 and 4f 5/2 electron levels of Bi^{3+} ions. After being reduced in KBH_4 solution, in addition to the binding energy peaks of Bi^{3+} ions discussed above, there are two peaks with binding energy of 157.2 eV and 162.5 eV can be observed in the pattern of Bi/BiOCl, corresponding to the 4f 7/2 and 4f 5/2 electron levels of metallic Bi, confirming the effective reduction in KBH_4 solution. The following oxidation results in the disappearance of binding energy peaks of metallic Bi and only the peaks of Bi^{3+} ions can be observed, indicating that the metallic Bi are oxidized to Bi^{3+} ions completely in the oxidation process.

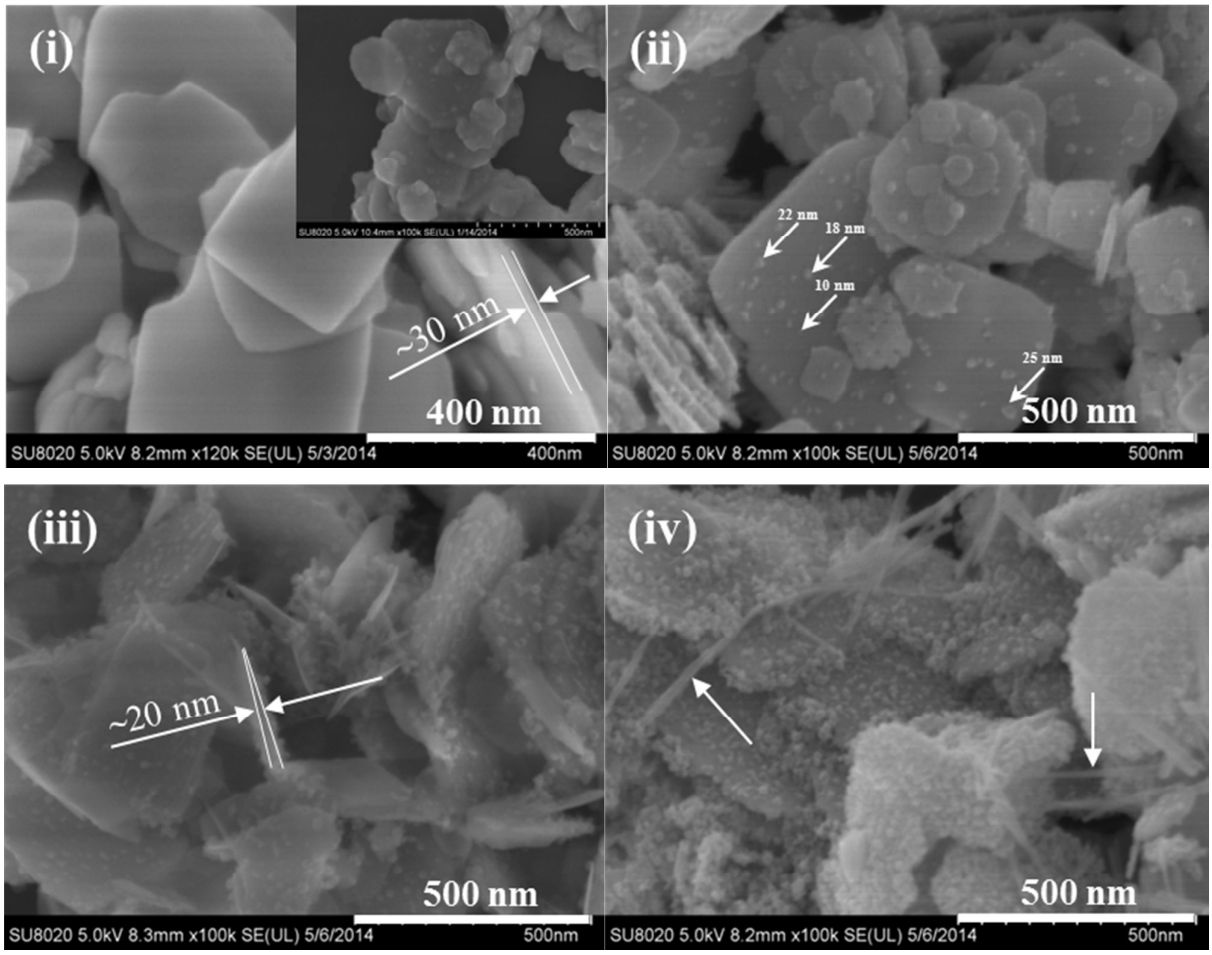

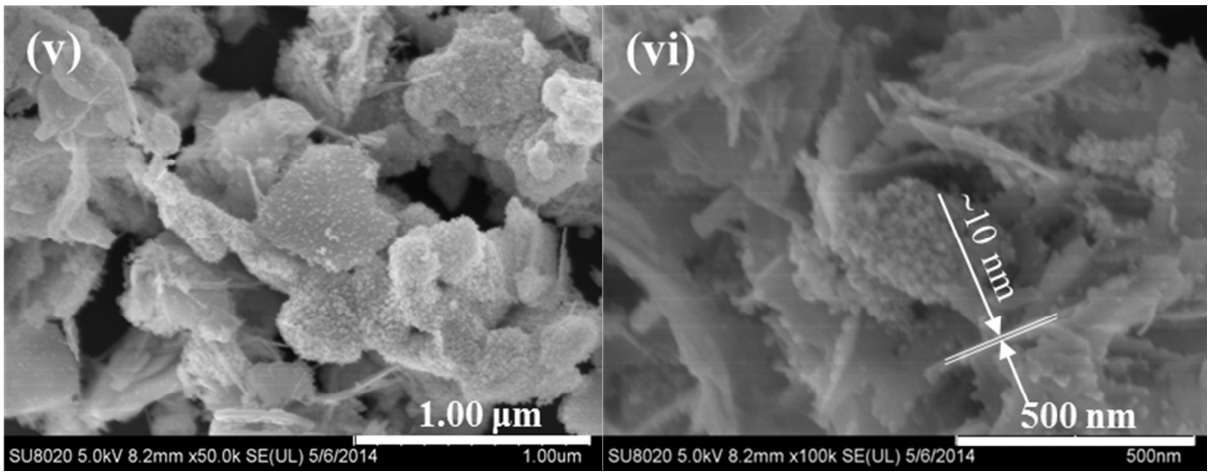

Fig.3 SEM morphologies of as-prepared BiOCl and Bi_2O_3/BiOCl prepared in KBH_4 solution with different concentrations, (i) BiOCl, inset is the BiOCl after being reduced in 0.02 M KBH_4 solution, (ii) Bi_2O_3/BiOCl-0.01, (iii) Bi_2O_3/BiOCl-0.02, (iv) Bi_2O_3/BiOCl-0.03, (v) Bi_2O_3/BiOCl-0.04 and (vi) Bi_2O_3/BiOCl-0.05

Fig.3 shows the SEM morphologies of as-prepared BiOCl and Bi_2O_3/BiOCl prepared in KBH_4 solutions with different concentrations. Fig.3 (i) is the morphology of BiOCl without modification. The as-prepared BiOCl powder is mainly composed of nanosheets with 300~500 nm in width and approximately 30 nm in thickness, and the surface of BiOCl nanosheets is quite smooth. The morphology of BiOCl reduced in 0.02 M KBH_4 solution is shown in the top right inset of Fig.3 (i). Shape of the nanosheets turns to be irregular to some extent, and some nanosheets break into small pieces. The surface of nanosheets is no longer smooth and has some visible nanoparticles on it, which are metallic Bi particles as revealed by XRD and XPS analyses. The Bi_2O_3/BiOCl nanosheets synthesized with different KBH_4 concetrations are shown in Fig.3 (ii), Fig.3 (iii), Fig.3 (iv), Fig.3 (v) and Fig.3 (vi), respectively. The shape of Bi_2O_3/BiOCl-0.01 nanosheets is similar to that of BiOCl nanosheets with the similar thickness of about 30 nm. Some nanoparticles of Bi_2O_3 are distributed sporadically on the surface of BiOCl nanosheets as revealed by XRD and XPS analyses.

With the increase of KBH_4 concentration, the morphology of Bi_2O_3/BiOCl samples changes in two aspects. First, the thickness of BiOCl nanosheets in Bi_2O_3/BiOCl samples decreases with the increase of KBH_4 concentration. And BiOCl nanosheets tend to be biconvex lens in shape, as shown in Fig.3 (iii) and (iv). The thickness of Bi_2O_3/BiOCl-0.05 nanosheets is approximately 10 nm or less, which is much thinner than that of as-prepared BiOCl nanosheets. Second, the distribution and size of Bi_2O_3 nanoparticles in Bi_2O_3/BiOCl samples change. When KBH_4 concentration is 0.01 M, only a few Bi_2O_3 nanoparticles with size smaller than 25 nm distribute sporadically on the surface of BiOCl nanosheets. The amount of Bi_2O_3 nanoparticles increases with increasing KBH_4 concentration, but the size of nanoparticles remains unchanged except for some aggregation of the nanoparticles occurs in the Bi_2O_3/BiOCl sample synthesized with high KBH_4 concentration shown in Fig.3 (vi).

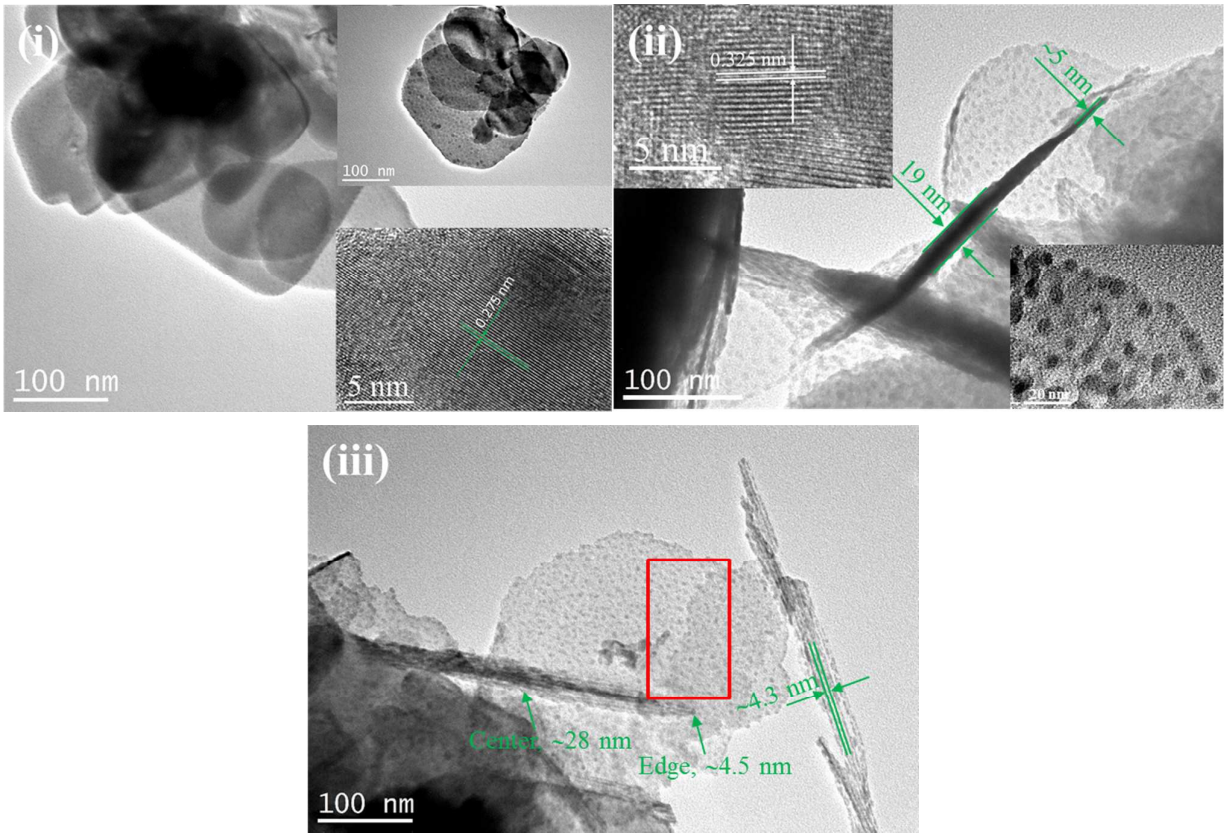

Fig.4 TEM morphologies of BiOCl and Bi_2O_3/BiOCl-0.02, (i) BiOCl nanosheets, bottom-right inset is the HRTEM view of BiOCl, top-right inset is the Bi modified BiOCl nanosheets; (ii) Bi_2O_3/BiOCl-0.02 nanosheets, bottom-right inset is an enlarged morphology of a Bi_2O_3/BiOCl nanosheet , top-left inset is the HRTEM view of Bi_2O_3 on BiOCl nanosheets; (iii) Bi_2O_3/BiOCl-0.02 nanosheets,

For further investigating the morphology of the samples, the TEM morphologies of as-prepared BiOCl and Bi_2O_3/BiOCl-0.02 are shown in Fig.4. Fig.4 (i) is the TEM morphology of as-prepared BiOCl nanosheets, demonstrating a smooth surface and a sheet width of several hundred nanometers. The HRTEM morphology of the nanosheets is shown in the bottom right inset. The lattice space is measured to be 0.275 nm, which corresponds to the (110) crystal plane of BiOCl. The morphology of BiOCl nanosheets after being reduced by 0.02 M KBH_4 solution is shown in the top right inset of Fig.4 (i). Which shows similar BiOCl nanosheets with a coarse surface caused by the deposited Bi nanoparticles on BiOCl nanosheets. The result is consistent with that reported in our previous work [22]. Fig.4 (ii) and (iii) are the morphologies of Bi_2O_3/BiOCl-0.02 nanosheets, on which BiOCl nanosheets modified with Bi_2O_3 nanoparticles can also be observed. Especially, the enlarged view of a BiOCl nanosheet shown in the bottom right inset in Fig.4 (ii) shows the evenly distributed Bi_2O_3 nanoparticles with a size of approximately 10 nm. The HRTEM view of the nanoparticle is shown in the top left inset in Fig.4 (ii), from which the lattice space is measured to be 0.325 nm, corresponding

to the (310) crystal plane of Bi_2O_3. In Fig.4 (ii), a nanosheet standing in the field of view shows clearly biconvex lens in shape with a center thickness of 19 nm and an edge thickness of approximately 5 nm, which is consistent with the SEM view in Fig.3 (iii). The hierarchical structure of BiOCl nanosheets in Bi_2O_3/BiOCl samples is seen very clearly when the nanosheets stand in the field of view, as shown in Fig.4 (iii). The interlaminar spacing can be measured to be approximately 4.3 nm. And this nanosheet is composed of 6 layers with each layer's thickness of approximately 25 nm. The hierarchical structure can also be differentiated on the flat side of the nanosheet with partly broken layers, as shown in the red box of Fig.4 (iii). Bi_2O_3 nanoparticles can be found not only on the surface of nanosheets, but also on the interface between layers of the laminated nanosheets. Therefore, it is believed that the Bi_2O_3/BiOCl nanosheets possess a hierarchical structure composed of several ultra-thin Bi_2O_3/BiOCl sub-sheets with a thickness of approximately 2 nm (half of the interlamellar spacing).

Fig.5 Schematic diagram of the hierarchical structure and forming process of Bi_2O_3/BiOCl heterojunctions

Fig.5 shows the schematic diagram of the hierarchical structure and forming process of Bi_2O_3/BiOCl heterojunctions. When being reduced in KBH_4 solution, the smooth surface of BiOCl nanosheets turns to be uneven by the forming of Bi nanoparticles. In consideration of that the reduction process of BiOCl nanosheets is an etching process, the Bi nuclei formed on the surface always grow inward to the nanosheets. Therefore, the mismatching between the crystal lattices of Bi and BiOCl results in the uneven surface with the embellishment of etching pits. Bi nanoparticles are further oxidized to Bi_2O_3 in the H_2O_2 solution. The oxidation in situ of Bi and rapid reaction speed produce the even distribution of Bi_2O_3 nanoparticles. Therefore, the hierarchical Bi_2O_3/BiOCl nanosheet composed of several ultra-thin sub-sheets can be obtained, which possesses high surface area and well-built junctions between Bi_2O_3 nanoparticles and BiOCl nanosheets.

3.2 Optical absorption performance

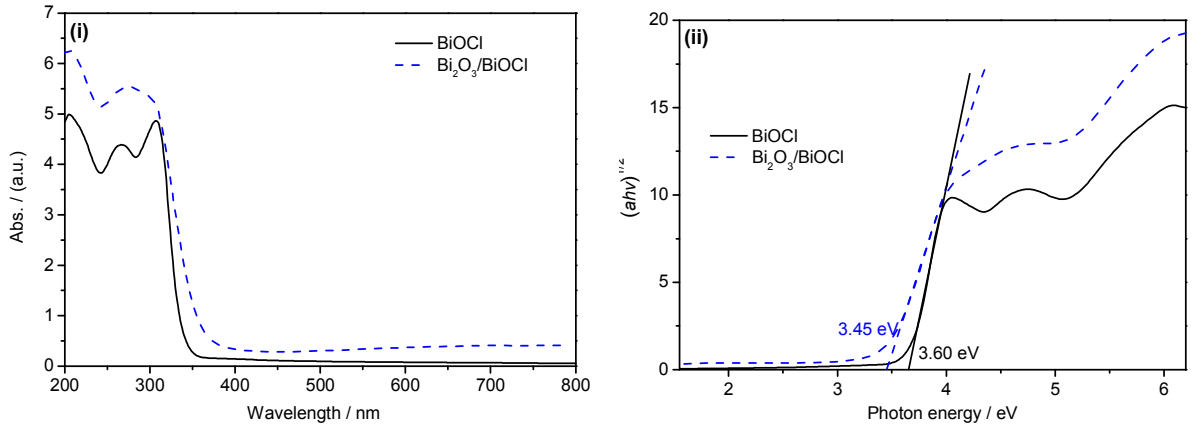

Fig.6 UV-Vis absorption spectra (i) and transformed Kubelka-Munk function vs. photon energy curves (ii) of BiOCl and Bi_2O_3/BiOCl nanosheets.

Optical absorption is the first step of the photocatalytic process, and is the key factor for the photocatalytic performance. The absorption edge and absorption intensity determine the efficiency of usage to the light illumination. UV-Vis diffuse reflectance spectrum (DRS) is an effective method to characterize the optical absorption performance of semiconductor samples.

Fig.6 shows the UV-Vis absorption spectra (i) and the transformed Kubelka-Munk function vs. photon energy curves (ii) of BiOCl, Bi_2O_3/BiOCl nanosheets with the optical wavelength ranging from 200 to 800 nm. BiOCl nanosheets possess a strong absorption in the UV region with the absorption edge at approximately 330 nm, and is optical absorption inert in the visible light region. The absorption intensity of Bi_2O_3/BiOCl nanosheets is higher than that of BiOCl, and the absorption edge of Bi_2O_3/BiOCl nanosheets shifts a little to the long wavelength direction compared with that of BiOCl nanosheets. There is a continuous low absorption in the whole visible light region for Bi_2O_3/BiOCl nanosheets, corresponding to the color change of samples from white to light yellow after being modified with Bi_2O_3 nanoparticles.

The band gaps of BiOCl samples can be estimated from the plot of $(\alpha h\upsilon)^{1/2}$ versus photon energy ($h\upsilon$) as shown in Fig.6(ii). The intercepts of the tangent to the x-axis give a good approximation of the band gap for the BiOCl and Bi_2O_3/BiOCl samples. The estimated band gap of the BiOCl nanosheets is approximately 3.6 eV, while the band gap of Bi_2O_3/BiOCl-0.02 nanosheets is approximately 3.44 eV, which is narrower than that of BiOCl nanosheets due to the introduction of semiconductor of Bi_2O_3.

3.3 Photocatalytic performance

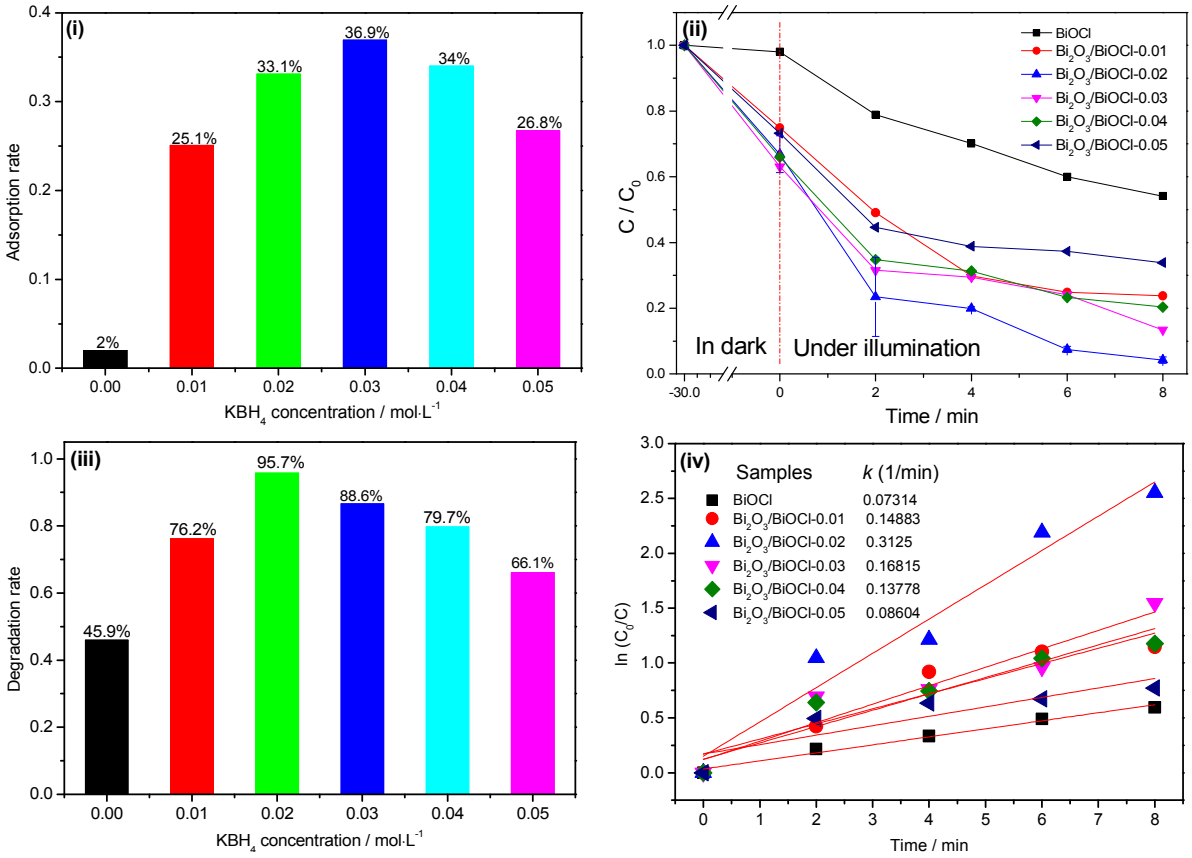

Fig.7 Photocatalytic performance of as-prepared BiOCl and Bi_2O_3/BiOCl samples synthesized with different KBH_4 concentrations on the degradation of MO with an initial concentration of 40 mg/L, (i) adsorption rate of 30 min, (ii) photodegradation curve, UV light, (iii) degradation rate, time of 8 min, (iv) photocatalytic kinetics analysis

Fig.7 shows the photocatalytic performance of as-prepared BiOCl and Bi_2O_3/BiOCl samples synthesized with different KBH_4 concentrations. The photocatalytic process is a surface reaction, and the adsorption performance of photocatalysts often determines their photocatalytic performance. Fig.7 (i) shows the adsorption performance of BiOCl, Bi_2O_3/BiOCl-0.01, Bi_2O_3/BiOCl-0.02, Bi_2O_3/BiOCl-0.03, Bi_2O_3/BiOCl-0.04 and Bi_2O_3/BiOCl-0.05 samples, respectively. As-prepared BiOCl sample with smooth surface possess relative poor adsorption performance with an adsorption rate of 2% in 30 min. All the adsorption rates of Bi_2O_3/BiOCl samples are much higher than that of BiOCl. The adsorption rate of Bi_2O_3/BiOCl samples increases initially with the increase of KBH_4 concentration, and achieves the highest adsorption rate of 36.9% at the KBH_4 concentration of 0.03 $mol \cdot L^{-1}$, but further increase of KBH_4 concentration decreases the adsorption rate, to 26.8% at the KBH_4 concentration of 0.05 M, though which is still much higher than that of BiOCl.

A key factor affecting the adsorption performance is the surface area of samples. The surface area of Bi_2O_3/BiOCl-0.02 powder is 32.1 m^2/g, which is almost twice that of BiOCl(18.1 m^2/g). The nanoparticles on the surface of BiOCl nanosheets and the hierarchical structure contribute to the

increase of the surface area. However, the big difference between the ratio of adsorption rates(~1:19.5) and that of surface area (~1:1.8) of BiOCl to Bi_2O_3/BiOCl powders indicates that surface area is probably not the only factor to affect the adsorption. The surface structure of Bi_2O_3 nanoparticles and the hierarchical structure of nanosheets may contribute to the adsorption performance.

Fig.7 (ii) shows the degradation curve (C/C_0 versus the degradation time) of different samples under UV light illumination, in which C is the remnant MO concentration after being degraded with given time, and C_0 is the initial MO concentration. In our previous work, BiOCl nanosheets showed excellent photocatalytic performance and achieve a degradation rate of 90% on a 20 mg/L MO solution in 8 min [22]. Here, the initial MO concentration increases to 40 mg/L and the MO concentration decreases approximately by half after being photodegraded by as-prepared BiOCl nanosheets for 8 min. All of the degradation curves of Bi_2O_3/BiOCl samples are below than that of BiOCl sample, indicating that all Bi_2O_3/BiOCl samples possess better photocatalytic property than that of as-prepared BiOCl sample. The Bi_2O_3/BiOCl-0.02 nanosheets show the best photocatalytic performance, which degrade the 40 mg/L MO completely in 8 min. The synthesis and the photocatalytic test of the Bi_2O_3/BiOCl-0.02 nanosheets are repeated for 4 times, and the error bars are also shown in this figure. Although the photocatalytic data in 2 min show relative high error, all the four samples can degrade the MO in 8 min with error less than 0.01.

The real degradation rates of all samples after being degraded for 8 min are shown in Fig.7 (iii). The abscissa gives the KBH_4 concentration and the null means as-prepared BiOCl sample. The degradation rate of as-prepared BiOCl sample is 45.9% and increases evidently with Bi_2O_3 nanoparticles modification.

The enhancement of photocatalytic performance may be ascribed to the existence of Bi_2O_3 nanoparticles and the hierarchical structure of nanosheets. For Bi_2O_3/BiOCl-0.01 sample, the similar shape of nanosheets with that of BiOCl leaves only the sporadical Bi_2O_3 nanoparticles, effect on promoting the photocatalytic performance, which achieves a degradation rate of 76.2%. The Bi_2O_3/BiOCl-0.02 sample achieves the highest degradation rate of 95.7% due to the synergistic effect of Bi_2O_3 nanoparticles and hierarchical structure. Further increase of KBH_4 concentration will decreases the degradation rates to 88.6% for the Bi_2O_3/BiOCl-0.03 sample, 79.7% for the Bi_2O_3/BiOCl-0.04 sample and 66.1% for the Bi_2O_3/BiOCl-0.05 sample. From the SEM views in Fig.3, thinner nanosheets are obtained for Bi_2O_3/BiOCl samples prepared in higher KBH_4 concentrations, which means higher surface areas are beneficial for the photocatalytic performance.

However, more Bi_2O_3 nanoparticles are formed and aggregated on the surface of BiOCl nanosheets, which would deteriorate the photocatalytic property of the samples. The combination of these two factors would give the explanation of that the photocatalytic performance of Bi_2O_3/BiOCl composites enhances initially and then reduces with the increasing KBH_4 concentration.

The photocatalytic degradation kinetics can be described by pseudo-first-order reaction as the following equation[23]:

$$\ln \frac{C_0}{C} = kt \quad (1)$$

Where k is the apparent reaction rate constant, and t is the irradiation time. The plot of $\ln(C_0/C)$ versus t can be obtained by converting the photocatalytic degradation data, and the slope of the linear fitting curves is the value of k. The converted kinetics plots are shown in Fig.7 (iv) and the k values of different samples are shown in the inset. All k values of Bi_2O_3/BiOCl samples are higher than that of as-prepared BiOCl sample (0.07314 1/min) and the Bi_2O_3/BiOCl-0.02 sample achieves the highest k value of 0.3125 1/min, which is four times that of as-prepared BiOCl sample. In consideration of the initial MO concentration (C_0), volume of the MO solution (V) and the quantity of catalysts (m), the photocatalytic ability can be defined as the quantity of photodegraded MO per unit time and unit quantity of catalysts, and can be calculated to be 0.0125 mg/(mg·min) according to the following equation:

$$\text{Photocatalytic ability} = k \cdot C_0 \cdot V/m \quad (2)$$

3.4 Photocatalytic mechanism

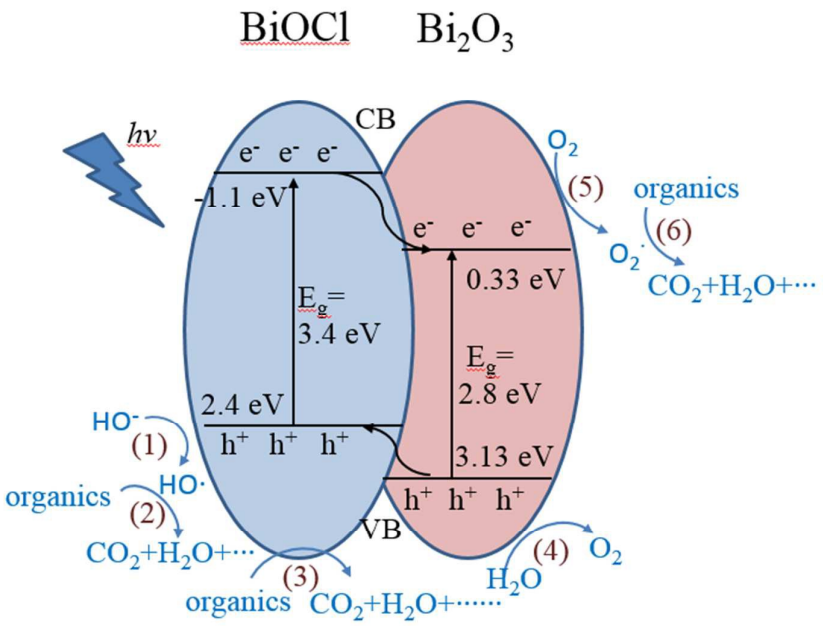

Fig.8 Schematic diagram of photocatalytic process of Bi_2O_3/BiOCl nanosheets

The in situ reduction and oxidation of the BiOCl nanosheets result in the hierarchical structure and Bi_2O_3 nanoparticles modification, which can enhance the photocatalytic performance of BiOCl nanosheets from several aspects, such as optical absorption, surface adsorption, chargers transfer and catalytic reactions. The optical absorption and surface adsorption have been discussed above, after being modified with Bi_2O_3 nanoparticles Bi_2O_3/BiOCl composite has a higher optical absorption intensity in UV region and higher MO adsorption. Especially, the main wavelength of the light source at 365 nm is very near to the band gap of Bi_2O_3/BiOCl composite, resulting in the extra absorption compared to as-prepared BiOCl nanosheets. Here, the transfer of photogenerated electron-hole pairs and the catalytic reactions during the photocatalytic process will be discussed and a schematic diagram of the photocatalytic process of Bi_2O_3/BiOCl nanosheets is shown in Fig.8.

When excited by UV light with the energy higher than the band gap, the transition of electrons from valence band (VB) to conduction band (CB) of BiOCl generates electron-hole pairs. Photogenerated electrons and holes will transfer to the surface of BiOCl, and part of them will recombine by emitting photons. The recombination is one of the key factors deteriorates the performance of the photocatalysts. Several methods can be applied to reduce the recombination rate during the charges transfer, such as ultra-thin structure [24], single crystalline structure and heterojunctions structure.

BiOCl nanosheets possess excellent photocatalytic performances due to the single crystalline structure. The hierarchical structure of BiOCl nanosheets with several ultra-thin sub-sheets of several nanometers in thickness would restrict the recombination rate due to the shorter charge transfer route, and enhance the photocatalytic performance. Furthermore, well combined Bi_2O_3/BiOCl heterojunctions result in the transfer of photogenerated electrons and holes between Bi_2O_3 and BiOCl. As shown in Fig.8, the CB of BiOCl (-1.1 eV, vs. NHE) is more negative than that of Bi_2O_3 (0.33 eV), when coupling well dispersed Bi_2O_3 nanoparticles with BiOCl nanosheets. The space charge layer at Bi_2O_3-BiOCl junctions accelerates the transfer of electrons from CB of BiOCl to CB of Bi_2O_3. The VB of Bi_2O_3 (3.13 eV) is more positive than that of BiOCl (2.4 eV), the holes from VB of Bi_2O_3 will transfer to that of BiOCl. Hence, the different transfer directions of the photogenerated electrons and holes result in the charges separation, low recombination rate and high photocatalytic performance.

The photocatalytic reaction on the surface of Bi_2O_3/BiOCl nanosheets can be described as follows:

$$OH^- + h^+ \rightarrow HO\cdot \quad (3)$$

$$\text{Organics} + HO\cdot \rightarrow \ldots\ldots \rightarrow CO_2 + H_2O + \ldots\ldots \quad (4)$$

$$\text{Organics} + h^+ \rightarrow \ldots\ldots \rightarrow CO_2 + H_2O + \ldots\ldots \quad (5)$$

$$H_2O + h^+ \rightarrow \ldots\ldots \rightarrow \text{dissolved } O_2 \quad (6)$$

$$e^- + O_2 \rightarrow \cdot O_2^- \quad (7)$$

$$\text{Organics} + \cdot O_2^- \rightarrow \ldots\ldots \rightarrow CO_2 + H_2O + \ldots\ldots \quad (8)$$

There are three active species, the hydroxyl radical (HO·), holes (h^+) and superoxide radicals ($\cdot O_2^-$) in the photocatalytic process, which can degrade the organics into CO_2, H_2O and other inorganic substances, as shown in reaction (4), (5) and (8), respectively. HO· radical forms when the h^+ is captured by OH^-, and the $\cdot O_2^-$ radical forms when the e^- is captured by dissolved O_2 in the solution. In order to clarify the role of the three active species in the photocatalytic process, three sacrificial agents were added in the MO solution to restrict the formation of corresponding active species, such as NaI for h^+, BQ for $\cdot O_2^-$ and IPA for HO·. Fig.9 shows the photocatalytic performance of BiOCl and Bi_2O_3/BiOCl nanosheets to the MO solutions with the addition of different sacrificial agents.

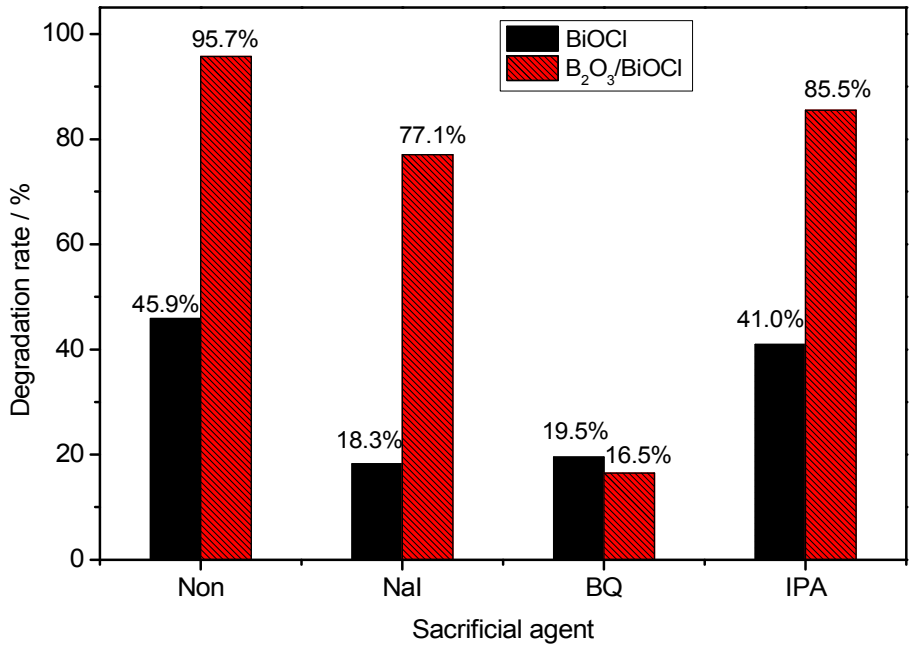

Fig.9 Photocatalytic performance of as-prepared BiOCl and Bi_2O_3/BiOCl nanosheets to the MO solutions with the addition of different sacrificial agents, the concentration of all added sacrificial agents is 10 mM.

For BiOCl nanosheets, when h^+ and $\cdot O_2^-$ radicals are restricted respectively the degradation rates decreases from 45.9% to 18.3% and 19.5%, indicating that h^+ and $\cdot O_2^-$ radicals would play a dominant role in the photocatalytic process. When IPA is added in the MO solution, the

photocatalytic rate decreases only 4.9% indicating that HO· radicals would play a secondary role in the photocatalytic process. In our previous work [22], the HO· concentrations of BiOCl and TiO_2 under illumination have been compared. The HO· concentration of BiOCl is much lower than that of TiO_2 in precondition of similar photocatalytic performance of the two samples, indicating that the HO· is not the main active species of BiOCl during the photocatalytic process. Here, this result is confirmed again.

However, the degradation rate changes are much different for Bi_2O_3/BiOCl nanosheets. Only 18.6% and 10.2% decrements of the degradation rate appear when the h^+ and HO· radicals are restricted respectively, and the decrement of degradation rate is 79.2% when $\cdot O_2^-$ radicals are captured by BQ. The $\cdot O_2^-$ radicals (related to photogenerated electrons) play a dominant role on the photocatalytic performance, and the h^+ and HO· radicals (related to photogenerated holes) play a secondary role. In consideration of that the photogenerated electrons and holes are equivalent in quantity, part of the holes may take part in the reaction of oxygen evolution by reaction (6), and the dissolved O_2 captures an electron to form $\cdot O_2^-$ radical. This process would be confirmed by the fact that the degradation rate changes little when N_2 is pumped continuously to maintain a N_2 ambient in the photocatalytic process.

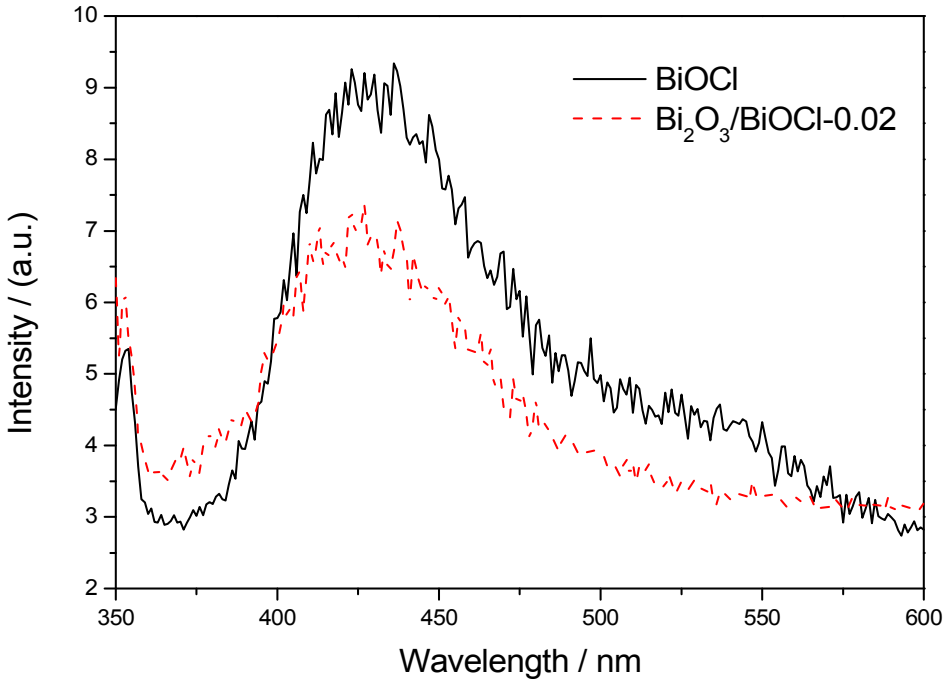

Fig.10 Photoluminescence patterns of terephthalic acid after being illuminated under UV light with BiOCl and Bi_2O_3/BiOCl-0.02 nanosheets, irradiation time of 15 min.

Concentrations of HO· radicals during photocatalytic process of BiOCl and Bi_2O_3/BiOCl-0.02 nanosheets were determined by terephthalic acid oxidation method. The emission intensities of

dihydroxyterephthalic acid reflect the HO· concentrations. The photoluminescence patterns of terephthalic acid solution after being illuminated under UV light for 15 min with BiOCl and Bi_2O_3/BiOCl-0.02 nanosheets are shown in Fig.10. The low emission intensities indicate low HO· concentrations of BiOCl and Bi_2O_3/BiOCl-0.02 nanosheets produced during photocatalytic process. The further decrease of emission intensity after Bi_2O_3 modification indicates lower HO· concentrations of Bi_2O_3/BiOCl-0.02 nanosheets during photocatalytic process.

The hierarchical structure of Bi_2O_3/BiOCl nanosheets and the photogenerated charge transfer on Bi_2O_3-BiOCl heterojunctions result in the enhancement of photocatalytic performance. The photogenerated electrons on the surface of Bi_2O_3 nanoparticles play the dominant role in the photocatalytic process by forming $\cdot O_2^-$ radicals and the photogenerated holes take part in this reaction through providing dissolved O_2, in addition to the direct oxidation to from HO· radicals.

4 Conclusions

BiOCl nanosheets were synthesized by the solvothermal method and modified by in situ reduction and oxidation in KBH_4 and H_2O_2 solutions respectively. Bi_2O_3 nanoparticles are evenly distributed on BiOCl nanosheets with sizes ranging from 10 to 25 nm. The BiOCl nanosheets are in a hierarchical structure with interlaminar spacing of approximately 4.3 nm, and the biconvex lens structure of BiOCl nanosheets composed of several ultrathin layers can be observed. The hierarchical Bi_2O_3/BiOCl nanosheets possess higher surface area and much higher adsorption rate than that of as-prepared BiOCl nanosheets. The hierarchical Bi_2O_3/BiOCl nanosheets show also higher photocatalytic performances than that of BiOCl nanosheets, and the Bi_2O_3/BiOCl-0.02 sample achieves the highest photodegradation rate of 93.6% in 8 min under UV light illumination. The enhancement of the photocatalytic performance of Bi_2O_3-BiOCl can be ascribed to several aspects, including higher surface area, higher UV light absorption rate and separation of photogenerated electron-hole pairs. The photogenerated electrons on Bi_2O_3 nanoparticles play the dominant role on the photocatalytic process by forming $\cdot O_2^-$ radicals, and the photogenerated holes take part in this reaction through providing dissolved O_2.

Acknowledgements

This work was supported by Nature Science Foundation of China (51102071, 51172059 and 51272063), Fundamental Research Funds for the Central Universities (2013HGQC0005), and Nature Science Foundation of Anhui Province (1408085QE86).

References

[1] L. Ye, Y. Su, X. Jin, H. Xie and C. Zhang, *Environ. Sci.: Nano*, 2014, 1, 90.

[2] J. Jiang, K. Zhao, X. Xiao and L. Zhang, *J. Am. Chem. Soc.*, 2012, 134, 4473.

[3] J. Xiong, G. Cheng, G. Li, F. Qin and R. Chen, *RSC Adv.*, 2011, 1, 1542.

[4] Y. Wang, Z. Shi, C. Fan, X. Wang, X. Hao and Y. Chi, *J. Solid State Chem.*, 2013, 199, 224.

[5] X. Qin, H. Cheng, W. Wang, B. Huang, X. Zhang and Y. Dai, *Mater. Lett.*, 2013, 100, 285.

[6] K.L. Zhang, C.M. Liu, F.Q. Huang, C. Zheng and W.D. Wang, *Appl. Catal., B*, 2006, 68, 125.

[7] C. F. Guo, S. Cao, J. Zhang, H. Tang, S. Guo, Y. Tian and Q. Liu, *J. Am. Chem. Soc.*, 2011, 133, 8211.

[8] H. Cheng, B. Huang and Y. Dai, *Nanoscale*, 2014, 6, 2009.

[9]X. Lin, T. Huang, F. Huang, W. Wang and J. Shi, *J. Phys. Chem. B*, 2006, 110, 24629.

[10] H. Li, L. Zhang, *Nanoscale*, 2014, 6 (14), 7805.

[11] K. Zhao, L. Zhang, J. Wang, Q. Li, W. He and J. Yin, *J. Am. Chem. Soc.,* 2013, 135, 15750.

[12] L. Ye, L. Zan, L. Tian, T. Peng and J. Zhang, *Chem. Commun.*, 2011, 47, 6951.

[13] J. Cheng, C. Wang, Y. Cui, Y. Sun, Y. Zuo and T. Wang, *Mater. Lett.*, 2014, 127, 28.

[14] D. Sun, J. Li, Z. Feng, L. He, B. Zhao, T. Wang, R. Li, S. Yin and T. Sato, *Cataly. Commun.*, 2015, 51, 1.

[15] C. Wang, C. Shao, Y. Liu and L. Zhang, *Scripta Mater.*, 2008, 59, 332.

[16] H. Liu, L. Ding, Z. Pei, Y. Zhou, J. Long, W. Deng and X. Wang, *Appl. Catal. B-Environ.,* 2014, 160-161, 98.

[17] W.J. Kim, D. Pradhan, B.K. Min, Y. Sohn, *Appl. Catal. B-Environ.*, 2014, 147, 711.

[18] W. Xiong, Q. Zhao, X. Li, D. Zhang, *Catal. Commun.*, 2011, 16, 229.

[19] X. Wang, Q. Wang, F. Li, W. Yang, Y. Zhao, Y. Hao and S. Liu, *Chem. Eng. J.*, 2013, 234, 361.

[20] W. Yang, B. Ma, W. Wang, Y. Wen, D. Zeng and B. Shan, *Phys. Chem. Chem. Phys.*, 2013, 15, 19387

[21] H. Cheng, B. Huang, X. Qin, X. Zhang and Y. Dai, *Chem. Commun.*, 2012, 48, 97.

[22] J. Hu, G. Xu, J. Wang, J. Lv, X. Zhang, Z. Zheng, Y. Wu. *New J. Chem.*, 2014, 38, 4913.

[23] H. Al-Ekabi, N. Serpone, *J. Phys. Chem*. 1988, 92, 5726.

[24] M. Guan, C. Xiao, J. Zhang, *J. Am. Chem. Soc.*, 2013, 135, 10411.

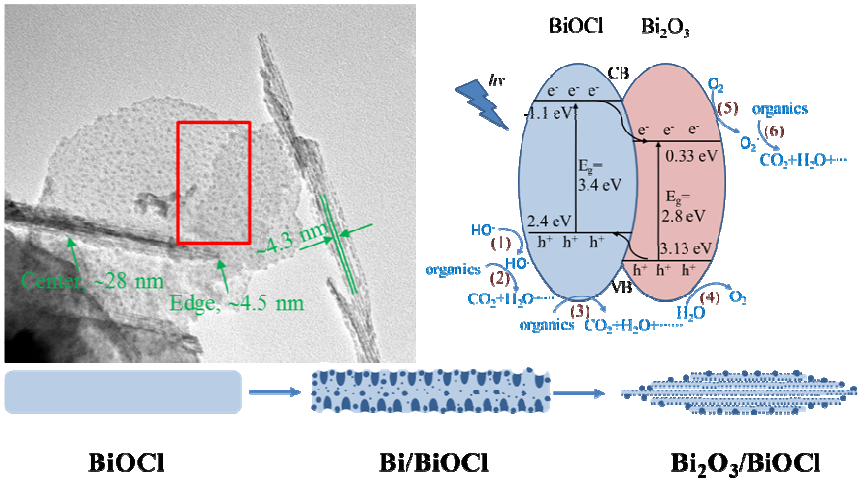

Bi_2O_3 nanoparticle modified BiOCl nanosheets with a nanolayered hierarchical structure synthesized by in situ reactions possess higher photocatalytic performance than that of BiOCl nanosheets.

Graphical Abatract: